

Supplementary Material

A Novel Pyridinium Functionalized Fluorenone Compound for Neutral Aqueous Organic Redox Flow Batteries

Wenjin Li; Jiayao Li; Xianzhi Yuan; Zhipeng Xiang*; Zhenxing Liang; Zhiyong Fu*.

Key Laboratory on Fuel Cell Technology of Guangdong Province, School of Chemistry and Chemical Engineering, South China University of Technology, Guangzhou 510641, P. R. China

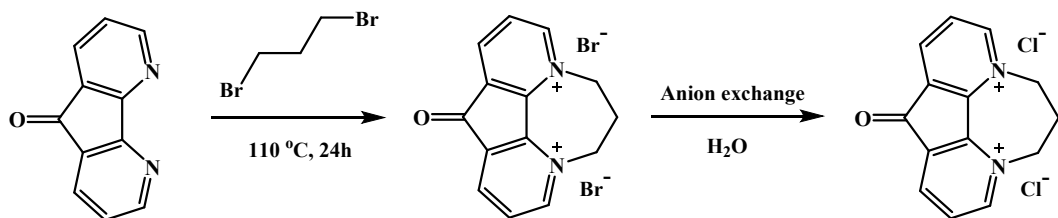
Table of contents	Page
Experimental section	S3-S5
Fig. S1. UV-Vis standard curve of (OTDFL)Cl ₂ .	S6
Fig. S2. A summary of different organic electroactive materials for aqueous organic redox flow batteries.	S7
Fig. S3. ¹ H NMR spectrum (a) and ¹³ C NMR spectrum (b) of (OTDFL)Cl ₂ (D ₂ O).	S8
Fig. S4. ¹ H NMR spectra of CDO (a) and (OTDFL)Cl ₂ (b) (DMSO-d ₆).	S9
Fig. S5. LSVs of 1.0 mM CDO and (OTDFL)Cl ₂ in 0.50 M NaCl with 0.10 M phosphate buffer solution (pH = 6.0).	S10
Fig. S6. Pourbaix diagram of the (OTDFL)Cl ₂ reduction processes.	S11
Fig. S7. (a) CVs of (OTDFL)Cl ₂ in 0.50 M NaCl with 0.10 M phosphate buffer solution (pH = 6.0) at different scan rates; (b) Nicholson analysis for the reduction processes.	S12
Fig. S8. TD-DFT simulated UV-Vis-absorption spectra.	S13
Fig. S9. ¹ H NMR spectrum of two (OTDFL) ⁺ -H (D ₂ O).	S14
Fig. S10. DFT calculations of binding free energy in two (OTDFL) ⁰ hydrogenation structures.	S15
Fig. S11. ¹ H NMR spectrum of (TPABPy)Cl ₃ (D ₂ O, quenched by phenylhydrazine).	S16
Fig. S12. Charge and discharge curves at different cycles with 1.6 and 0.3 V cut-offs.	S17
Fig. S13. Cycling performance of 1.0 M (OTDFL)Cl ₂ -(TPABPy)Cl ₃ at 20 mA cm ⁻² ; (b) charge and discharge profiles of 1.0 M (OTDFL)Cl ₂ at different cycles.	S18
Fig. S14. (a) ¹ H NMR spectra of 0.25 M electrolyte after 250-cycle test and under buffer solution (D ₂ O, pH=8.0).	S19
Table S1. Related physicochemical properties of CDO and (OTDFL)Cl ₂ .	S20
Table S2. Summary of reported organic electroactive materials in Fig. S2.	S21
References	S22-S23

Experimental section

1. Reagents and materials

5H-cyclopenta[2,1-b:3,4-b']dipyridin-5-one (Innochem Co., Ltd., China), 1,3-dibromopropane (Aladdin Reagent Co., Ltd., China), Amberlite IRA-900 (Cl, Alfa Aesar Co., Ltd., China), sodium chloride (NaCl), sodium dihydrogen phosphate (NaH₂PO₄), Sodium hydrogen phosphate (Na₂HPO₄), sodium hydroxide (NaOH), phosphoric acid (H₃PO₄) (Guangzhou Chemical Reagent Factory, China) both are analytical reagent and used as received without further treatment. All the solutions were prepared with ultrapure water (Milli-Q reference, R>18.2 MΩ.cm).

2. Synthesis of (OTDFL)Cl₂



Scheme S1. Synthesis protocol.

4-oxo-4,8,9,10-tetrahydro-7a,10a-diaza-cyclohepta-[def]fluorene-7a,10a-dium chloride (OTDFL)Cl₂ is synthesized by the addition reaction between 5H-cyclopenta[2,1-b:3,4-b']dipyridin-5-one (CDO) and 1,3-dibromopropane. Briefly, in a 250 mL flask, a mixture solution of CDO (30.0 g, 0.16 mol) and 1,3-dibromopropane (100 mL, 0.96 mol) was stirred at 110 °C for 24 h. After cooling to room temperature, the solid was filtered out and washed with acetone and hexanes, and then dried under vacuum to afford 4-oxo-4,8,9,10-tetrahydro-7a,10a-diaza-cyclohepta-[def]fluorene-7a,10a-dium bromine (OTDFL)Br₂ (49.0 g, 79.8%, black solid). Then, (OTDFL)Br₂ was treated with anion exchange to obtain purplish red solid (OTDFL)Cl₂ (35.8 g, 95.2%).

3. Ultraviolet-visible spectrum (UV-Vis) test

Ultraviolet-Visible (UV-Vis) spectra were collected on a Shimadzu UV-2600 spectrometer equipped with an optional integrating sphere.

4. Nuclear magnetic resonance (NMR) test

¹H NMR and ¹³C NMR spectra were conducted on an AVANCE III HD 500 MHz (Bruker, Germany) by solving the compound in deuterium reagents.

5. Electron paramagnetic resonance (EPR) test

EPR spectra were obtained using a Bruker ELEXSYS-II E500 CW-EPR (Bruker, Germany)

spectrometer equipped with nitrogen.

6. Electrochemical test

Cyclic voltammetry (CV) and linear sweep voltammetry (LSV) were performed on a CHI 730E electrochemical workstation. All electrochemical test systems added 0.50 M NaCl as a supporting electrolyte. The CVs were collected on a standard three-electrode system, with a glassy carbon disk (diameter of 3.0 mm) as the working electrode, an Ag/AgCl electrode as the reference electrode, and a platinum wire as the counter electrode. A homemade Au ultramicro electrode (UME, diameter of 25.0 μm) was used to collect the LSV. The analysis of the UME LSV was conducted via equation S1^[S1],

$$i_{ss} = \frac{4nFADC_0^*}{\pi r_0} = 4nFDC_0r_0 \quad (\text{S1})$$

where i_{ss} represents limiting current, n is the electron transfer number ($n= 2$), F is the Faraday constant (96485 C mol^{-1}), r_0 is the electrode radius ($12.5 \mu\text{m}$), C_0 is the bulk concentration of (OTDFL)Cl₂ (1.0 mM), and D is the diffusion coefficient ($\text{cm}^2 \text{ s}^{-1}$).

The electron transfer rate constant was determined by Nicholson's method (equation S2-S3),

$$\psi = (-0.6288 + 0.0021\Delta E_P)/(1 - 0.017\Delta E_P) \quad (\text{S2})$$

$$\psi = k^0[\pi DnF/RT]^{-1/2}v^{-1/2} \quad (\text{S3})$$

where ψ represents the dimensionless Nicholson parameter, ΔE_P is the difference between the cathode peak potential and anode peak potential, k^0 is the electron transfer rate constant (cm s^{-1}), R is the ideal gas constant ($8.314 \text{ J mol K}^{-1}$), T is the testing temperature (298 K), v is the scan rate (V s^{-1}).

7. Battery test

A laboratory-scale flow battery was assembled as follows. Graphite felt electrodes ($3.0 \text{ cm} \times 3.0 \text{ cm}$ in size, 4.0 mm thick) were placed beside the titanium current collectors. A Fumasep FAA-A-3-50 anion-exchange membrane was used as the separator. Negolyte and posolyte were circulated through the battery by a peristaltic pump (Longer BT100-2J) at a flow rate of 60.0 mL min^{-1} . The battery test was performed on a Neware BTS 3000 battery testing system at room temperature in a glove box (Universal 2440/750/900) with an argon atmosphere (99.999%). The posolyte used (TPABPy)Cl₃ as active species^[S2]. For all the battery tests, the negolyte volume was 5.0 mL and the posolyte volume was 6.0 mL. The battery was cycled by using the constant current-constant voltage (CC-CV) method. During charging, the voltage limits were set at 1.5 V with 20 mA cm^{-2} and 1.0 mA cm^{-2} cutoff current density.

During discharging, the voltage limits were set at 0.3 V with 20 mA cm⁻² and 1.0 mA cm⁻² cutoff current density.

8. Density functional theory (DFT) calculation

All DFT calculations were performed by using Gaussian 09 program^[S3]. The initial configurations were optimized at the (U)B3LYP/6-311G(d) level, including the empirical dispersion correction (GD3BJ)^[S4, S5] and the implicit solvation model based on density (SMD). All optimized structures were checked by harmonic vibrational frequencies to ensure that they were on the minima of the potential energy surface (imaginary frequency = 0). To simulate the UV-Vis absorption spectra, the low-lying vertical excitation energies were calculated by using TD-DFT. The spin density distribution of the optimized structure and TD-DFT electron excitation were analyzed by Multiwfn^[S6] and drawn by VMD^[S7] package. The binding free energies (BFE) between hydrogen proton and (OTDFL)⁰ were calculated using equation S4,

$$\text{BFE} = E_{[(\text{OTDFL})^+ \cdot \text{H}]} - E_{[(\text{OTDFL})^0]} - E_{(\text{H}^+)} \quad (\text{S4})$$

where $E_{[(\text{OTDFL})^+ \cdot \text{H}]}$, $E_{[(\text{OTDFL})^0]}$, and $E_{(\text{H}^+)}$ represent the sum of electronic and thermal free energies of (OTDFL)⁺-H, (OTDFL)⁰ and H⁺, respectively.

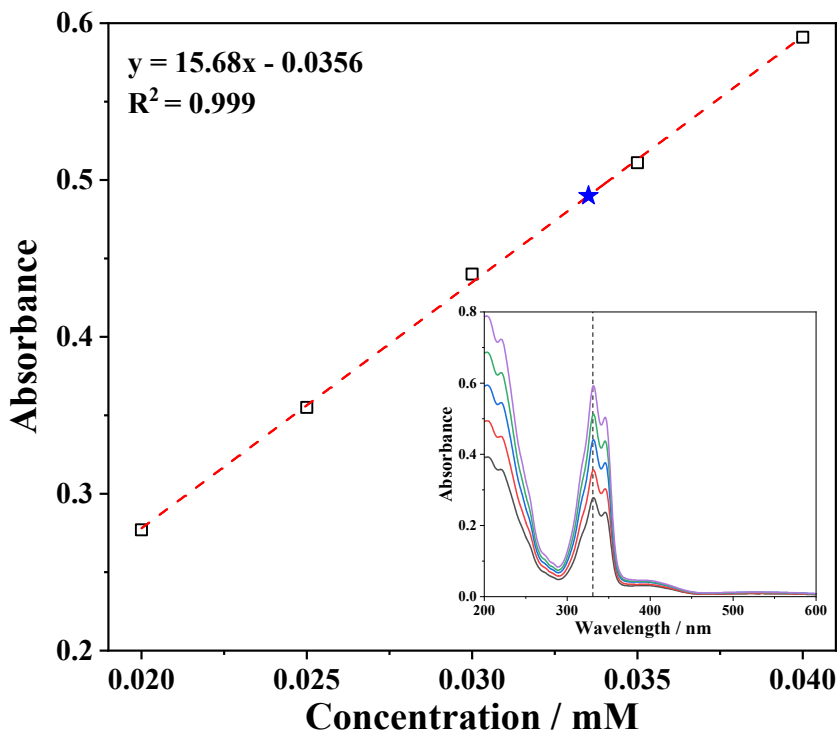


Fig. S1. UV-Vis standard curve of (OTDFL)Cl₂, the inset displays the UV-Vis spectra of (OTDFL)Cl₂ at different concentrations.

The above standard curve was established by plotting the concentrations versus absorbance, and the absorbance at 331 nm was used to quantify the concentration based on the Lambert-Beer law. The aqueous solubility of (OTDFL)Cl₂ was measured as follows. The saturated solution was diluted by 100000 times and the absorbance was collected (blue star dot). The saturated concentration (S) was calculated as

$$S = (0.49 + 0.0356) / 15.68 \times 100000 = 3352 \text{ mM} = 3.35 \text{ M.}$$

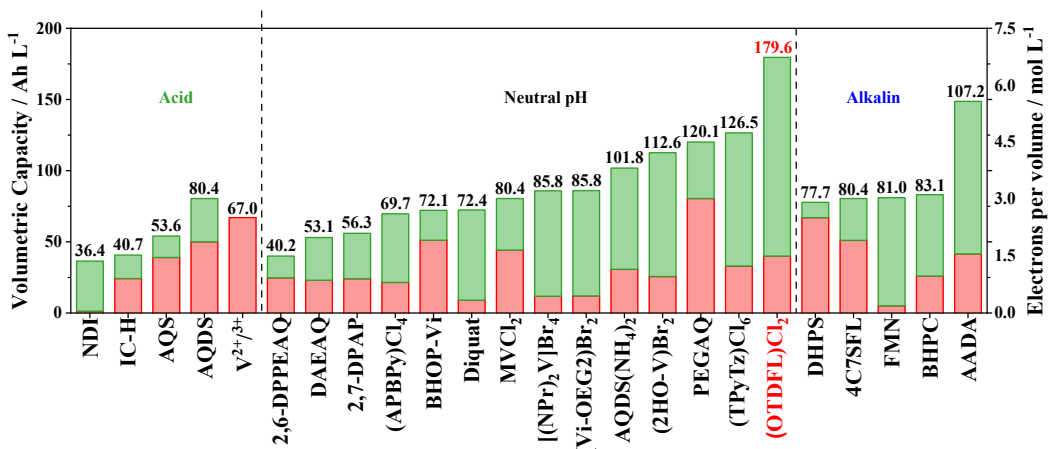


Fig. S2. A summary of different organic electroactive materials for aqueous organic redox flow batteries.

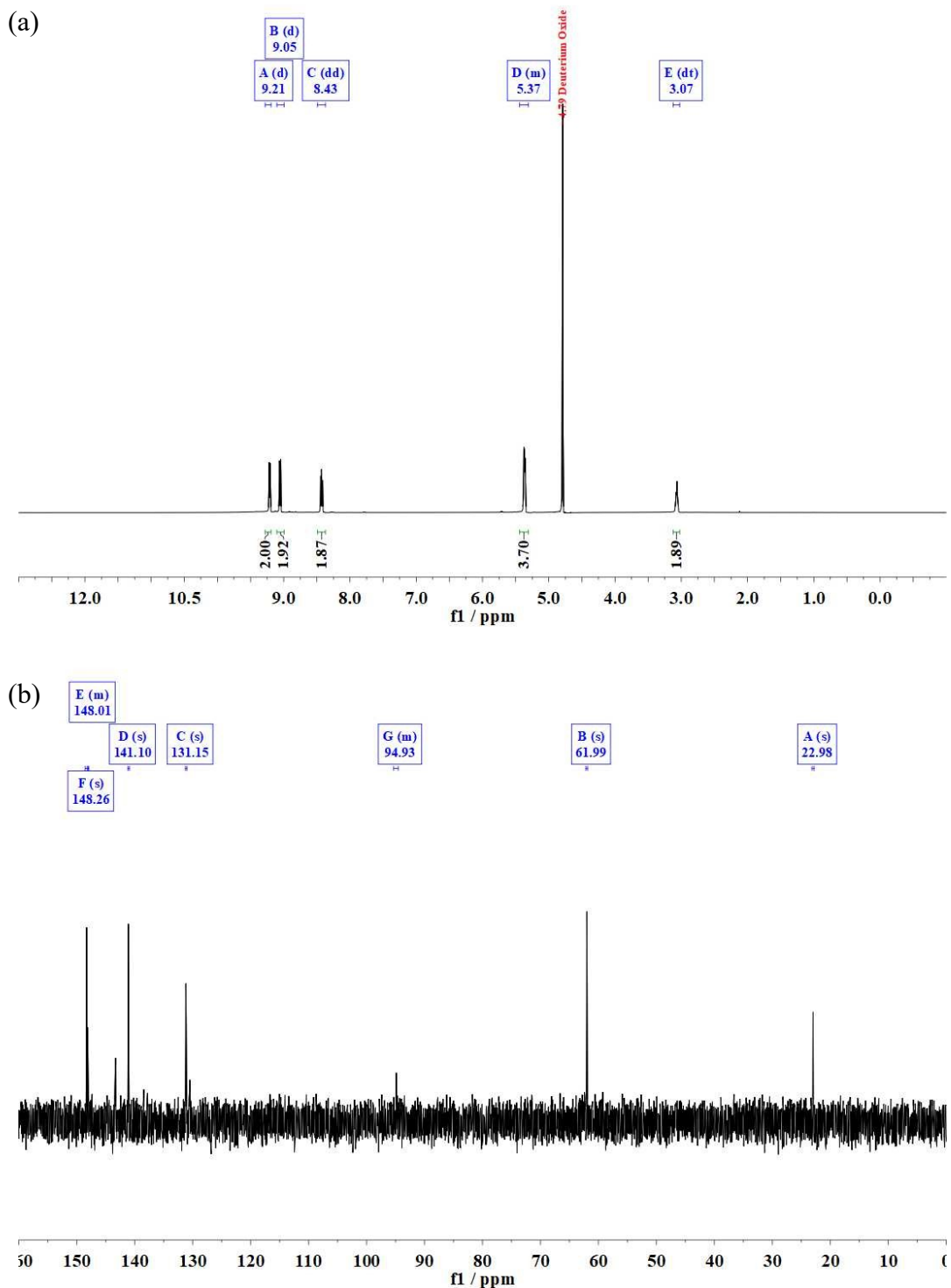


Fig. S3. ^1H NMR spectrum (a) and ^{13}C NMR spectrum (b) of $(\text{OTDFL})\text{Cl}_2$ (D_2O).

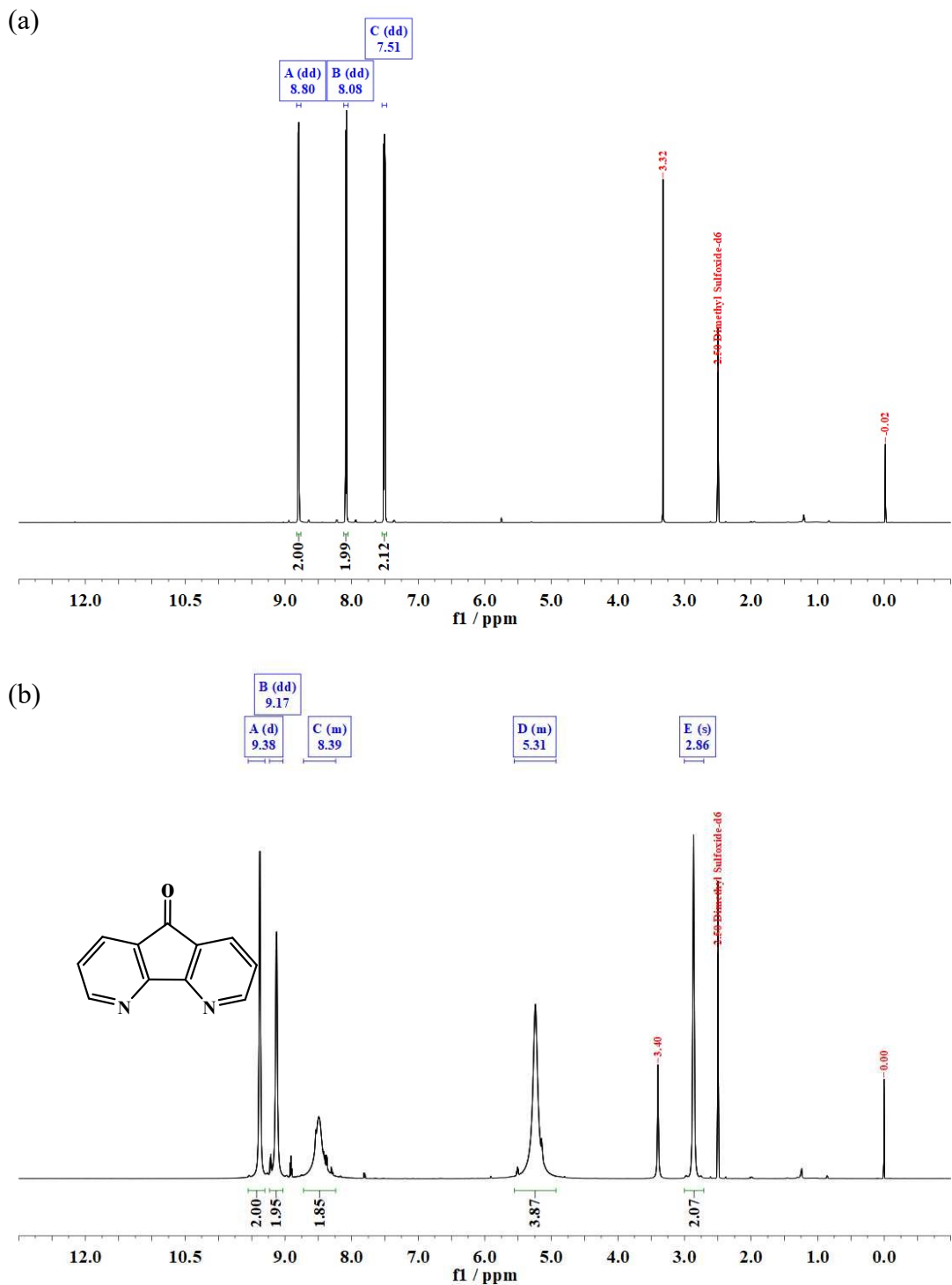
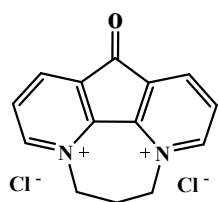


Fig. S4. ^1H NMR spectra of CDO (a) and $(\text{OTDFL})\text{Cl}_2$ (b) (DMSO-d_6).



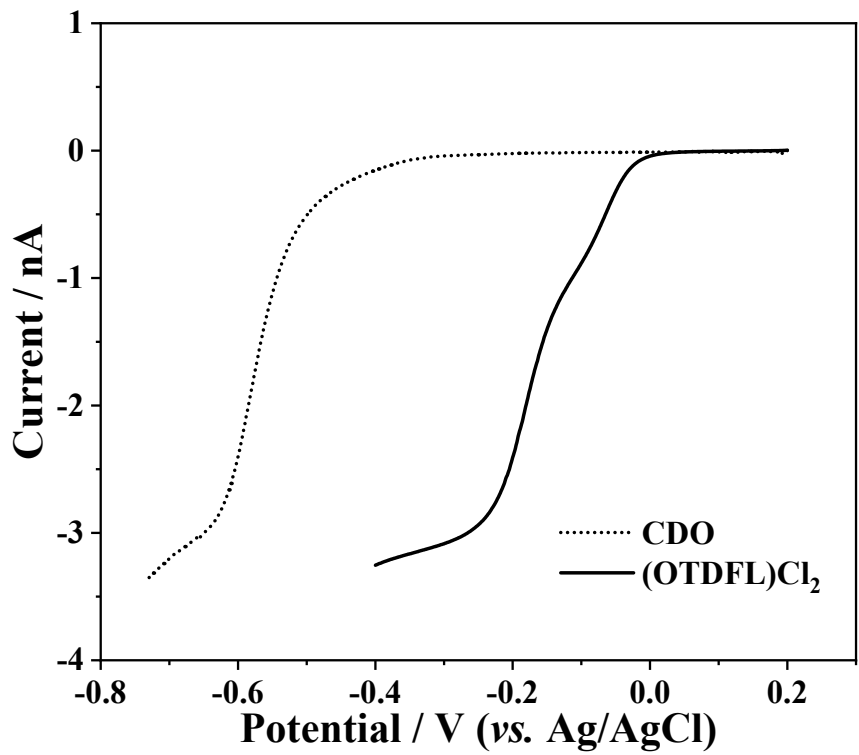


Fig. S5. LSVs of 1.0 mM CDO and (OTDFL)Cl₂ in 0.50 M NaCl with 0.10 M phosphate buffer solution (pH = 6.0).

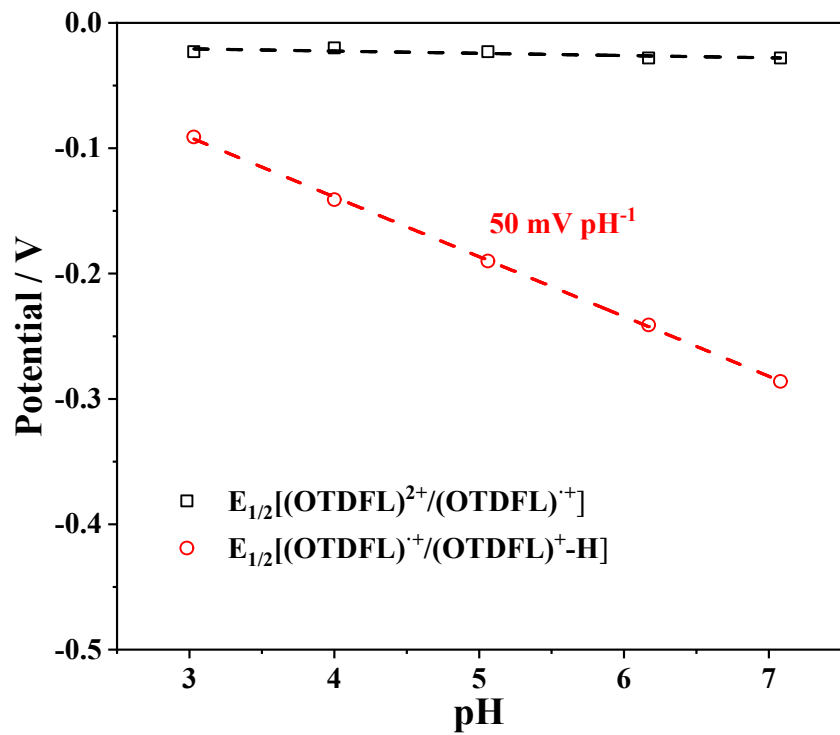


Fig. S6. Pourbaix diagram of the $(\text{OTDFL})\text{Cl}_2$ reduction processes.

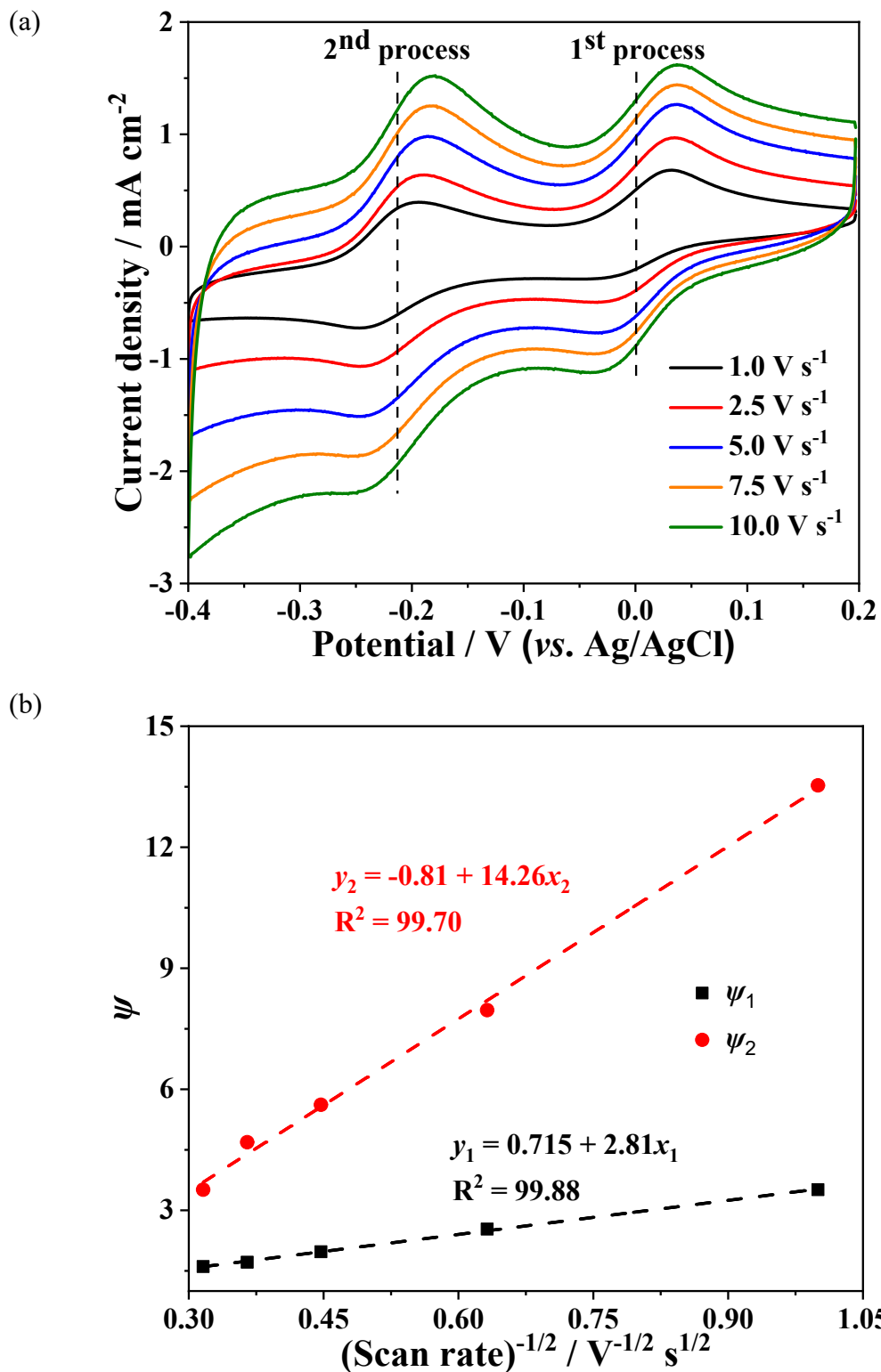


Fig. S7. (a) CVs of 1.0 mM (OTDFL)Cl₂ in 0.50 M NaCl with 0.10 M phosphate buffer solution (pH = 6.0) at different scan rates; (b) Nicholson analysis for the electrochemical processes of [(OTDFL)²⁺/(OTDFL)^{•+}] and [(OTDFL)^{•+}/(OTDFL)^{+-H}].

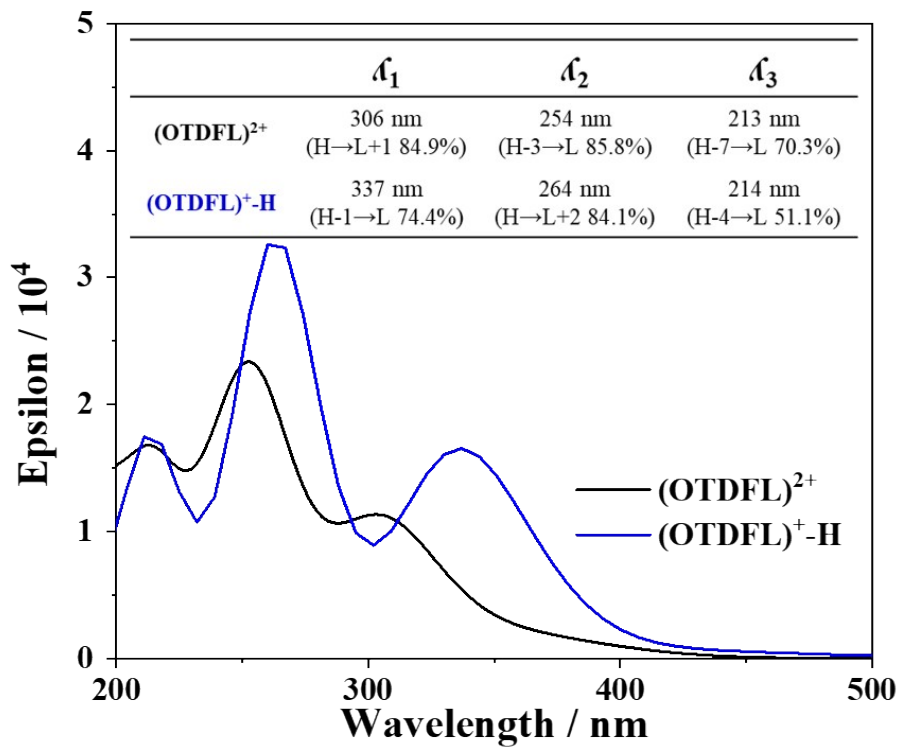


Fig. S8. TD-DFT simulated UV-Vis spectra (inset: main absorbance analysis; H represents the highest occupied molecular orbital (HOMO); L represents the lowest unoccupied molecular orbital).

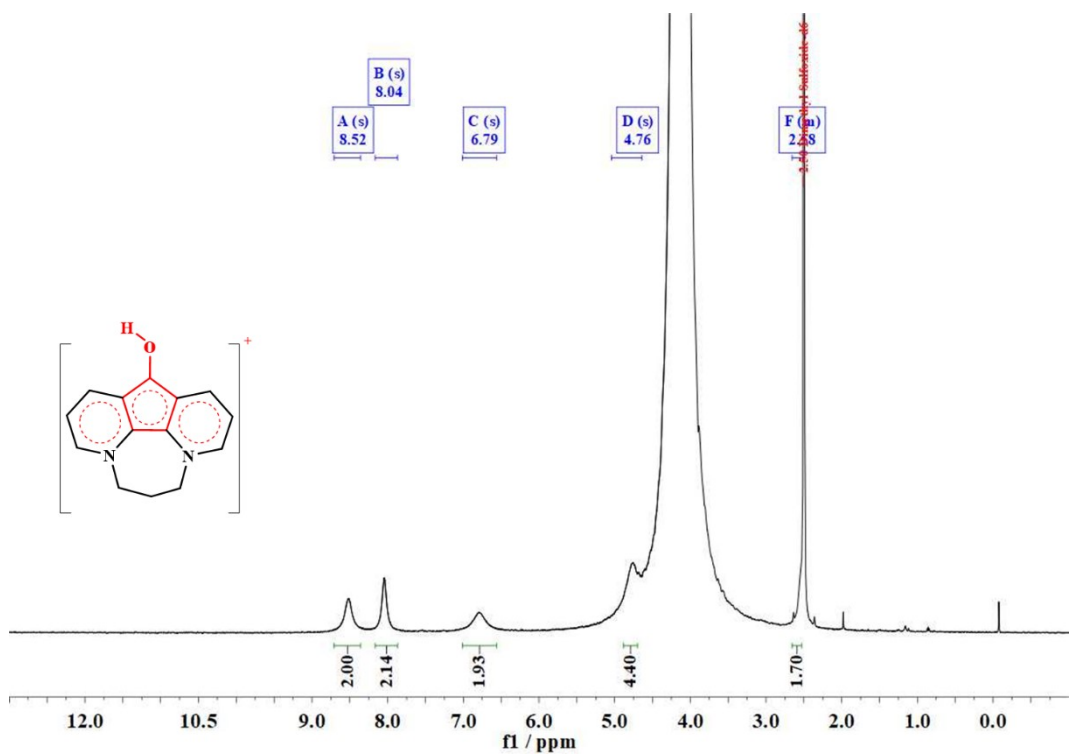


Fig. S9. ¹H NMR spectrum of two-electron reduced (OTDFL)Cl₂ [(OTDFL)⁺-H, D₂O].

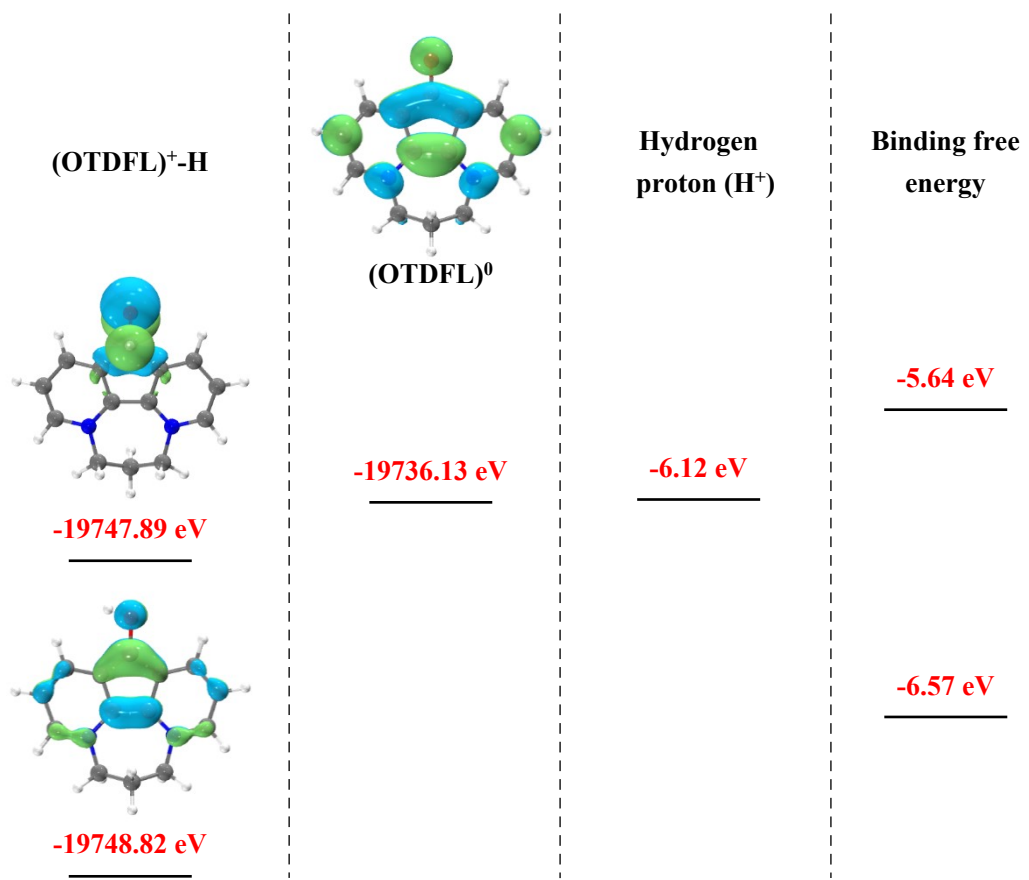


Fig. S10. DFT calculations of binding free energy with two $(OTDFL)^0$ hydrogenation structures.

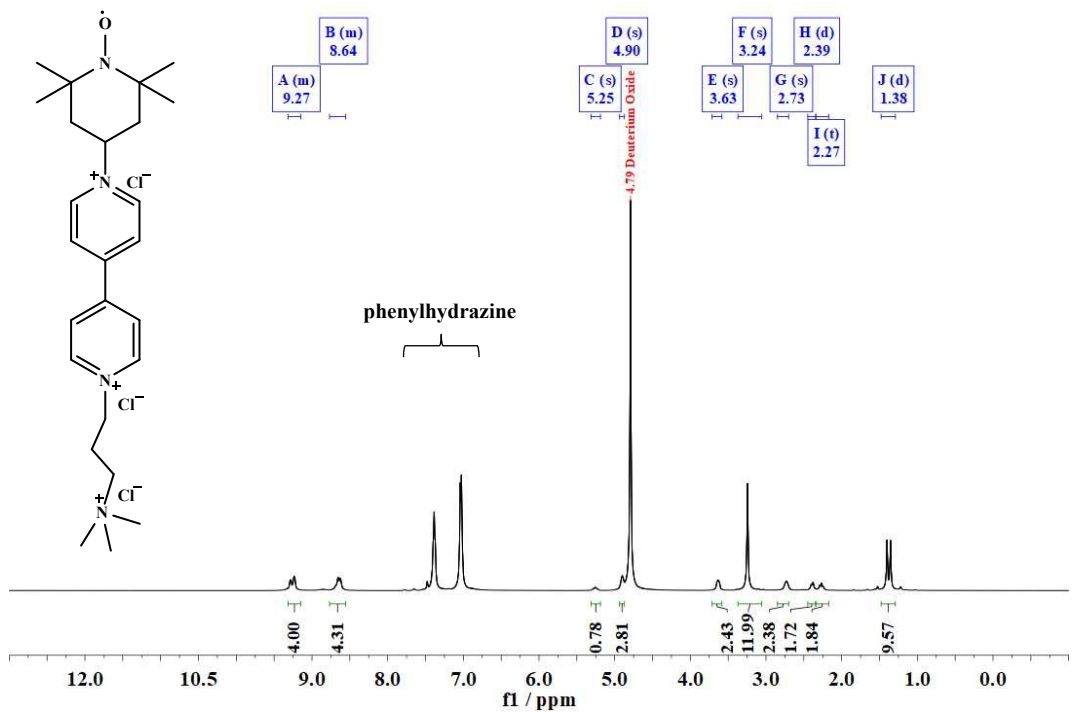


Fig. S11. ^1H NMR spectrum of $(\text{TPABPy})\text{Cl}_3$ (D_2O , quenched by phenylhydrazine).

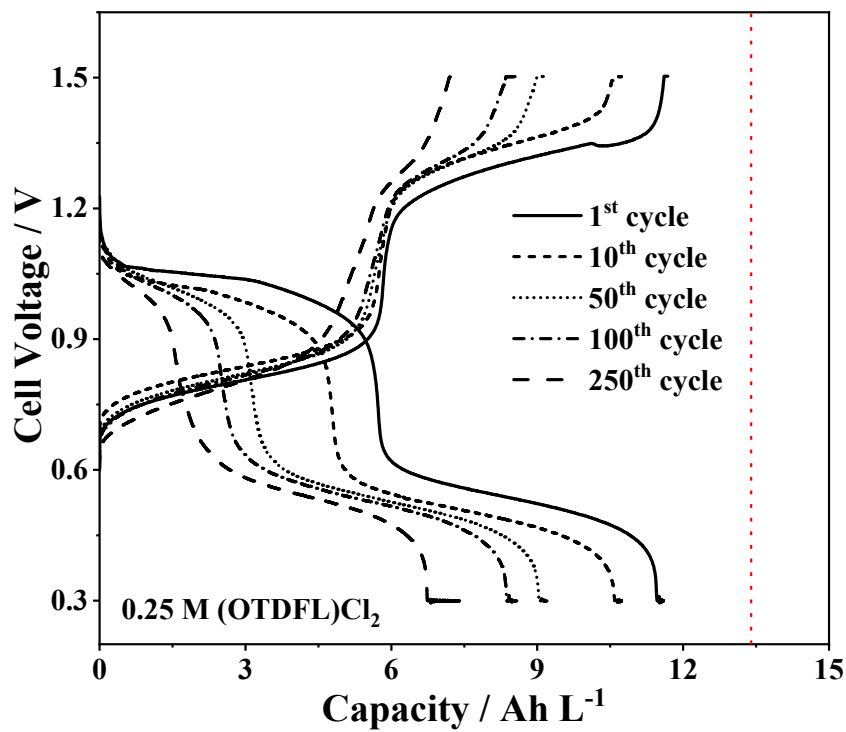


Fig. S12. Charge and discharge curves at different cycles with 1.5 and 0.3 V cut-offs (20 mA cm⁻¹, 0.25 M (OTDFL)Cl₂-(TPABPy)Cl₃ in pH = 6.0 buffer solution).

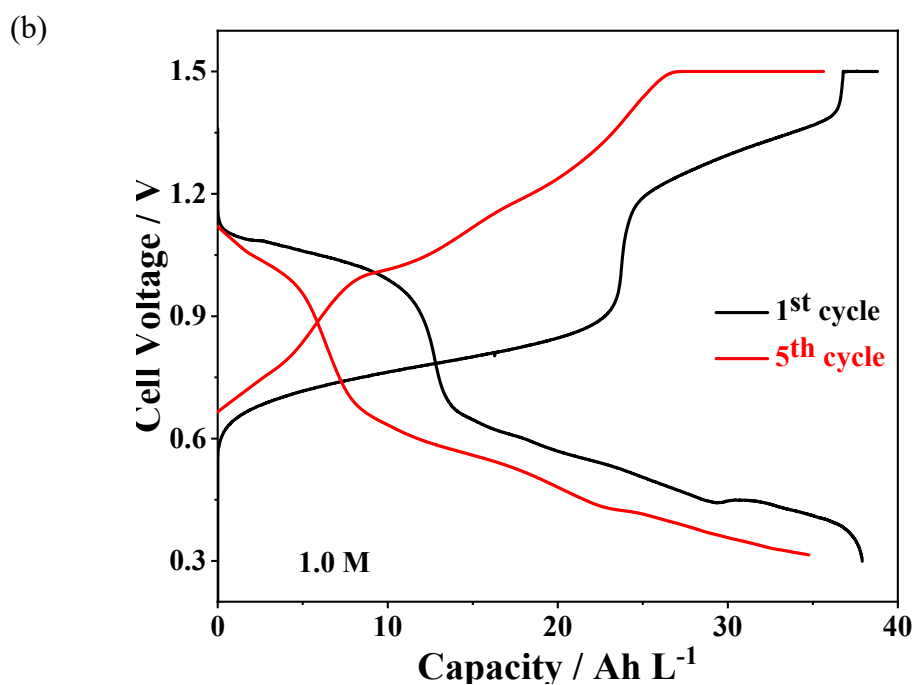
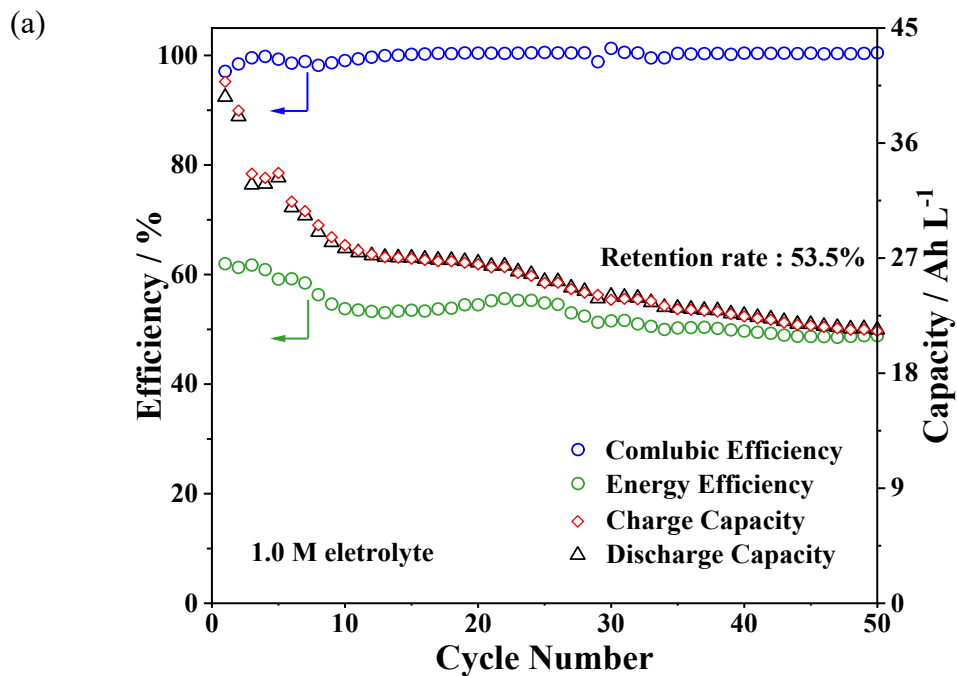


Fig. S13. (a) Cycling performance of 1.0 M (OTDFL)Cl₂-(TPABPy)Cl₃ at 20 mA cm⁻²; (b) charge and discharge profiles of 1.0 M (OTDFL)Cl₂ at different cycles.

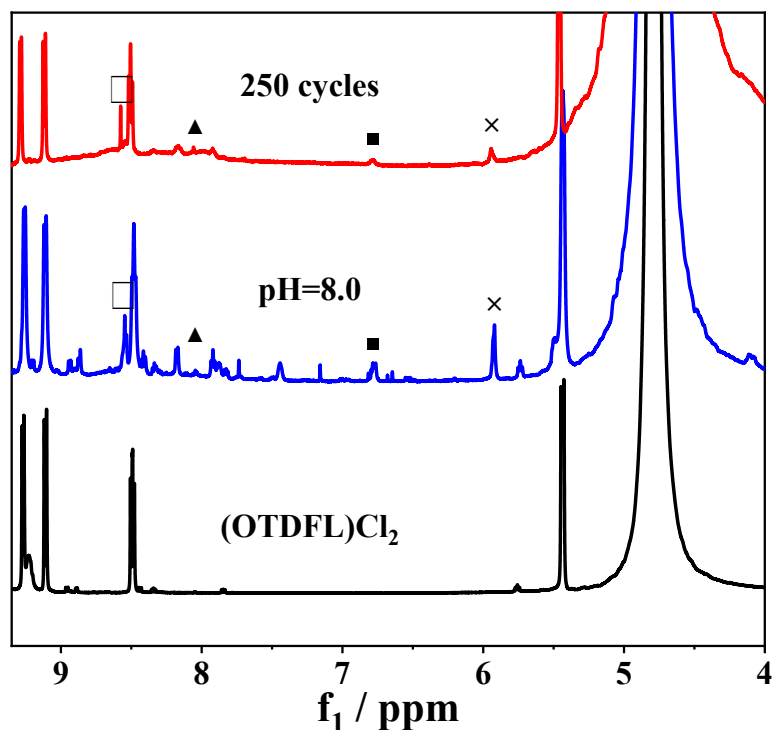


Fig. S14. ^1H NMR spectra of 0.25 M $(\text{OTDFL})\text{Cl}_2$ electrolyte after 250-cycle test and under 0.25 M buffer solutions (D_2O , $\text{pH}=8.0$).

Compound	Solubility (25 °C, g L ⁻¹)	Conductivity (1 mM, uS cm ⁻¹)	E_{1/2}(I⁺²/I⁺¹) (V, vs. Ag/AgCl)	E_{1/2}(I⁺¹/I⁰) (V, vs. Ag/AgCl)	Diffusion coefficient (Fig. S5, cm ² s ⁻¹)
CDO	<0.5	1.9	-0.60	- 1.10	6.44×10 ⁻⁶
(OTDFL)Cl ₂	610	216	-0.04	-0.29	3.19×10 ⁻⁶
KCl ^a	372	118	-	-	-

Table S1. Related physicochemical properties of CDO and (OTDFL)Cl₂

Name	Solubility [mol L ⁻¹ H ₂ O or electrolyte]	Molar mass [g mol ⁻¹]	Demonstrated concentration [mol L ⁻¹ H ₂ O or electrolyte]	Electron transferred per mol[mol]	Demonstrated Half-cell volumetric capacity [Ah L ⁻¹]	Theoretical Half-cell volumetric capacity [Ah L ⁻¹]
NDI ^[S8]	0.68	468.27	0.025	1	~1.32	36.4
IC-H ^[S9]	0.76 in 0.10 M HClO ₄	465.95	0.70	2	24.20	40.7
AQS ^[S10]	1.0 in 1.0 M H ₂ SO ₄	288.28	1.0	2	39.67	53.6
4A⁴⁺-NDI^[S11]	1.5	958.52	1.0	2	52.57	80.4
V ³⁺ /V ²⁺ ^[S12]	3.0	50.94	2.5	1	61.57	80.4
2,6-DPPEAQ^[S13]	0.75 (pH=9)	484.33	0.50	2	~24.72	40.2
DAEAQ^[S14]	0.99 (pH=12)	384.14	0.50	2	23.32	53.1
2,7-DPAP^[S15]	1.05	354.13	0.50	2	23.80	56.3
(APBPy)Cl ₄ ^[S16]	1.3	574.22	0.50	2	21.50	69.7
BHOP-Vi^[S17]	2.7	432.00	2.00	1	~51.11	72.1
Diquat^[S18]	2.7	369.97	0.50	1	~8.50	72.4
MVCI₂^[S19]	3.0	256.05	2.00	1	54.00	80.4
[(NPr)₂V]Br₄^[S20]	1.6	673.98	0.25	2	~11.40	85.8
(Vi-OEG2)Br₂^[S21]	1.6	522.22	0.50	2	12.0	85.8
AQDS(NH₄)₂^[S22]	1.9	404.03	0.75	2	30.70	101.8
(2HO-V)Br₂^[S23]	2.2	403.97	1.0	2	~39.66	112.6
PEGAQ^[S24]	2.24 (pure phase)	527.19	1.5	2	80.40	120.1
(TPyTz)Cl₆^[S25]	1.18	825.29	0.50	4	33.00	126.5
OTDFL (this work)	3.35	294.03	1.0	2	37.90	179.6
DHPS^[S26]	1.8 in 1.0 M KOH	292.27	1.4	2	67.00	77.7
4C7SFL^[S27]	1.3 in 2.0 M KOH	349.98	1.4	2	~52.77	80.4
FMN^[S28]	1.5 in 1.0 M KOH	478.09	0.24	1	5.03	81.0
BHPC^[S29]	1.55 in 1.0 M KOH	290.07	0.50	2	25.40	83.1
AADA^[S30]	2.0 in 2.0 M NaOH	379.34	0.80	2	41.50	107.2

Table S2. Summary of reported organic electroactive materials in Fig. S2

References

- [S1] J. E. Baur; R. M. Wightman, *J Electroanal. Chem.*, 1991, 305, 73-81.
- [S2] Hu, S.Z., Wang, L.W., Yuan, X.Z., Xiang, Z.P., Huang, M.B., Luo, P., Liu, Y.F., Fu, Z.Y., Liang, Z.X., *Energy Material Advances*, 2021, 9795237, 1-8.
- [S3] Gaussian 09, Revision A.02, M. J. Frisch, G. W. Trucks, D. J. Fox, et al. Gaussian, Inc., Wallingford CT, 2009.
- [S4] S. Grimme, S. Ehrlich, L. Goerigk, *J. Comput. Chem.*, 2011, 32, 1456–1465.
- [S5] S. Grimme, *J. Comput. Chem.*, 2004, 25, 1463–1473.
- [S6] T. Lu, F. W. Chen, *J. Comput. Chem.*, 2012, 33, 580–592.
- [S7] W. Humphrey, A. Dalke, K. Schulten, *J. Mol. Graphics*, 1996, 14, 3338.
- [S8] C. Wiberg, F. Owusu, E. Wang, E. Ahlberg, *Energy Technology*, 2019, 7, 1900843.
- [S9] A. Mukhopadhyay, H. Zhao, B. Li, J. Hamel, Y. Yang, D. Cao, A. Natan, H. Zhu, *ACS Appl. Energy Mater.*, 2020, 3, 7228.
- [S10] M. R. Gerhardt, L. Tong, R. Gomez-Bombarelli, Q. Chen, M. P. Marshak, C. J. Galvin, A. Aspuru-Guzik, R. G. Gordon, M. J. Aziz, *Adv. Energy Mater.*, 2017, 7, 1601488.
- [S11] V. Singh, S. Kwon, Y. Choi, S. Ahn, G. Kang, Y. Yi, M. Lim, J. Seo, M. Baik, H. R. Byon, *Adv. Mater.*, 2023, 2210859.
- [S12] L. Li, S. Kim, W. Wang, M. Vijayakumar, Z. Nie, B. Chen, J. Zhang, G. Xia, J. Hu, G. Graff, J. Liu, Z. Yang, *Adv. Energy Mater.*, 2011, 1, 394–400.
- [S13] Y. Ji, M.-A. Goulet, D. A. Pollack, D. G. Kwabi, S. Jin, D. De Porcellinis, E. F. Kerr, R. G. Gordon, M. J. Aziz, *Adv. Energy Mater.*, 2019, 9, 1900039.
- [S14] C. Wang, B. Yu, Y. Liu, H. Wang, Z. Zhang, C. Xie, X. Li, H. Zhang, Z. Jin, *Energy Storage Mater.*, 2021, 36, 417-426.
- [S15] S. Pang, X. Wang, P. Wang, Y. Ji, *Angew. Chem. Int. Ed.*, 2021, 60, 5289-5298.
- [S16] S. Hu, T. Li, M. Huang, J. Huang, W. Li, L. Wang, Z. Chen, Z. Fu, X. Li, Z. Liang, *Adv. Mater.*, 2021, 33, 2005839.
- [S17] Y. Liu, Y. Li, P. Zuo, Q. Chen, G. Tang, P. Sun, Z. Yang, T. Xu, *ChemSusChem*, 2020, 13, 2245-2249.
- [S18] J. Huang, Z. Yang, V. Murugesan, E. Walter, A. Hollas, B. Pan, R. S. Assary, I. A. Shkrob, X. Wei, Z. Zhang, *ACS Energy Lett.*, 2018, 3, 2533-2538.
- [S19] T. Janoschka, N. Martin, M. D. Hager, U. S. Schubert, *Angew. Chem. Int. Ed.*, 2016, 55, 14427-14430.
- [S20] C. DeBruler, B. Hu, J. Moss, X. Liu, J. Luo, Y. Sun, T. L. Liu, *Chem*, 2017, 3, 961-978.
- [S21] Y. Yao, W. Ma, J. Lei, Z. Wang, Y.-C. Lu, L. Liu, *J. Mater. Chem. A*, 2023, Advance Article. DOI: 10.1039/d2ta09177a.
- [S22] B. Hu, J. Luo, M. Hu, B. Yuan, T. Leo Liu, *Angew. Chem. Int. Ed.*, 2019, 58, 16629-16636.
- [S23] W. Liu, Y. Liu, H. Zhang, C. Xie, L. Shi, Y. G. Zhou, X. Li, *Chem. Commun.*, 2019, 55, 4801-4804.
- [S24] S. Jin, Y. Jing, D. G. Kwabi, Y. Ji, L. Tong, D. De Porcellinis, M.-A. Goulet, D. A. Pollack, R. G. Gordon, M. J. Aziz, *ACS Energy Lett.*, 2019, 4, 1342-1348.
- [S25] J. Huang, S. Hu, X. Yuan, Z. Xiang, M. Huang, K. Wan, J. Piao, Z. Fu, Z. Liang, *Angew. Chem. Int. Ed.*, 2021, 60, 20921-20925.
- [S26] A. Hollas, X. Wei, V. Murugesan, Z. Nie, B. Li, D. Reed, J. Liu, V. Sprenkle, W. Wang, *Nat. Energy*, 2018, 3, 508-514.

- [S27] R. Feng, X. Zhang, V. Murugesan, A. Hollas, Y. Chen, Y. Shao, E. Walter, N. P. N. Wellala, L. Yan, K. M. Rosso, W. Wang, *Science*, 2021, 372, 836–840.
- [S28] A. Orita, M. G. Verde, M. Sakai, Y. S. Meng, *Nat. Commun.*, 2016, 7, 13230.
- [S29] C. Wang, X. Li, B. Yu, Y. Wang, Z. Yang, H. Wang, H. Lin, J. Ma, G. Li, Z. Jin, *ACS Energy Lett.*, 2020, 5, 411-417.
- [S30] X. Zu, L. Zhang, Y. Qian, C. Zhang, G. Yu, *Angew. Chem. Int. Ed.*, 2020, 59, 22163-22170.